International Journal of Geo-Information

MDPI

Article

Watershed Land Cover/Land Use Mapping Using Remote Sensing and Data Mining in Gorganrood, Iran

Masoud Minaei [1,*] and Wolfgang Kainz [2]

[1] Department of Geography, Ferdowsi University of Mashhad, Mashhad 9177948974, Iran
[2] Department of Geography and Regional Research, University of Vienna, A-1010 Vienna, Austria; wolfgang.kainz@univie.ac.at
* Correspondence: m.minaei@um.ac.ir; Tel.: +98-935-547-1477

Academic Editors: Qiming Zhou, Zhilin Li and George P. Petropoulos
Received: 12 March 2016; Accepted: 22 April 2016; Published: 28 April 2016

Abstract: The Gorganrood watershed (GW) is experiencing considerable environmental change in the form of natural hazards and erosion, as well as deforestation, cultivation and development activities. As a result of this, different types of Land Cover/Land Use (LCLU) change are taking place on an intensive level in the area. This research study investigates the LCLU conditions upstream of this watershed for the years 1972, 1986, 2000 and 2014, using Landsat MSS, TM, ETM+ and OLI/TIRS images. LCLU maps for 1972, 1986, and 2000 were produced using pixel-based classification methods. For the 2014 LCLU map, Geographic Object-Based Image Analysis (GEOBIA) in combination with the data-mining capabilities of Gini and J48 machine-learning algorithms were used. The accuracy of the maps was assessed using overall accuracy, quantity disagreement and allocation disagreement indexes. The overall accuracy ranged from 89% to 95%, quantity disagreement from 2.1% to 6.6%, and allocation disagreement from 2.1% for 2014 to 2.7% for 2000. The results of this study indicate that a significant amount of change has occurred in the region, and that this has as a consequence affected ecosystem services and human activity. This knowledge of the LCLU status in the area will help managers and decision makers to develop plans and programs aimed at effectively managing the watershed into the future.

Keywords: GEOBIA; data mining; machine learning; Landsat

1. Introduction

Land Cover/Land Use (LCLU) change studies have become an essential part of current plans for dealing with environmental and natural resource management across the globe, both by national and local organizations [1]. As a result of population growth, agricultural and urban expansion, and a reduction in forest cover and rangelands, different types of LCLU change are taking place at an intensive level in developing countries [2,3]. Both [4] and [5] have confirmed the significant influence of LCLU change on the planet. LCLU change is a progressive, widespread and accelerating process, one driven mainly by anthropogenic derangements and natural phenomena, in turn driving changes that impact upon humans [6]. Humans play a major role as forces of change in the environment, imposing change at all levels, ranging from the global to the local [6]. In the Gorganrood watershed (GW), conditions are similar to those in other parts of the world. In 2006, and based on census statistics, about 600,000 people were living in six cities and more than 500 villages located across the GW area [7]. Therefore, to better understand environmental change and to identify the influence of LCLU changes on related events (for instance, natural hazards like floods, landslides), the use of LCLU maps can be seen as a necessary first step in the process [8].

Under these circumstances, LCLU change is now considered a major component of global environmental change, and thus an important field of research [9]. As a consequence, there has been a general effort made to develop reliable methods for identifying and monitoring LCLU changes [10]. Currently, it is widely accepted that LCLU change can be monitored at different scales using remote sensing (RS) satellite imagery [10], which has since become the most common data source for the detection, quantification and mapping of LCLU patterns and changes, due to its repetitive data acquisition, digital format suitable for computer processing, and accurate georeferencing procedures [11]. Monitoring and change detection using remote sensing requires the use of several multi-date (sometimes multi-sensor) images to evaluate the changes occurring in LCLU due to both environmental conditions and human actions, *i.e.* those that occur between images' acquisition dates [11].

Since the 1970s, multispectral remote-sensing images taken of Earth have been available from satellite systems and used widely in geographical studies encompassing LCLU mapping and change detection [8]. An adequate understanding of landscape phenomena, imaging properties and methodologies employed to extract information used in analysis is key to the successful use of satellite remote sensing in support of LCLU studies [11,12]. In light of these considerations, and based on the importance of the study area in terms of the agricultural products, residents, urban expansion activities and geohazards (e.g., floods) that exist there, a number of studies have already produced LCLU maps of the area. For example, In [13] author used artificial neural networks to provide LCLU maps and detect tree cover changes in Golestan province, Iran, using TM and ETM+ images from 1987 and 2001 to identify forest cover changes. Furthermore, [14] introduced a method to create accurate LCLU maps using ancillary data, while [15] provided a LULC map in 1998 for the Dough watershed (a small upstream sub-basin of the GW), for use in flood analysis. However, despite the global interest in LCLU change, few researchers have studied LCLU conditions in the Gorganrood region and only [13] investigated the LCLU changes, though exclusively in terms tree cover. Moreover, none of these research studies have covered the entire study area. In addition, they have not produced maps covering long periods of time; some have provided one land cover map or analyzed the changes taking place over only two points in time.

Therefore, given the importance of the landscape and the LCLU changes [16] taking place in the study area, plus the lack of understanding of the LCLU conditions and patterns over the last 40 years, our aim in this study was to analyze and quantify LCLU changes taking place in the GW. As part of this, a further aim was to carry out comprehensive LCLU mapping research, *i.e.*, to produce LCLU maps for the whole period using different Geographic Information Science (GIS) approaches, and also several historical and recent datasets. In this paper, we first classify the remote-sensing images obtained, then describe the LCLU changes that occurred between 1972 and 2014, and then characterize the major changes and conversions that have taken place.

2. Materials and Methods

Change detection studies use remote-sensing data as a crucial source of information [17], and classifying the images obtained is a key step in most LCLU analyses. In this regard, we used a number of different ways to classify the satellite images obtained for this study, as shown in Figure 1.

2.1. Study Area

The study area is located in the northeast of Iran and covers an area of 5500 km2 (Figure 2). It is located between the latitudes 36°57′N and 37°47′N, and the longitudes 55°08′E and 56°25′E, and contains the upstream parts of the GW. Altitudes in the area range between 15 and 2541 m above sea level. The area is very important for several reasons, including its agricultural production activities and fertile soils, and has a population of about 600,000 people [7]. It also contains the Golestan National Park, a UNESCO heritage site containing ancient forests, and a large range of flora and fauna species, some of which are endangered and might suffer due to any LCLU changes taking place there. The main

plant species of the region include the broadleaf *Fagus orientalis*, chestnut-leaved oak, *Carpinus betulus*, *Acer cappadocicum* and elm zelkova, *etc* [18]. In addition, this area enjoys agricultural products such as wheat, cotton, oil seeds, grains, *etc*. Moreover, the study area is geographically complex, and reveals large climatic variation. The plains are located in the east and center; to the south, the area is covered by dense forests and dry highlands, while the north mostly contains hills and is semi-arid [19]. For this study, the selected area was buffered using a 1.5 km distance and all the images were a subset of this buffer boundary. This buffer covered the entire study area to achieve a more accurate classification.

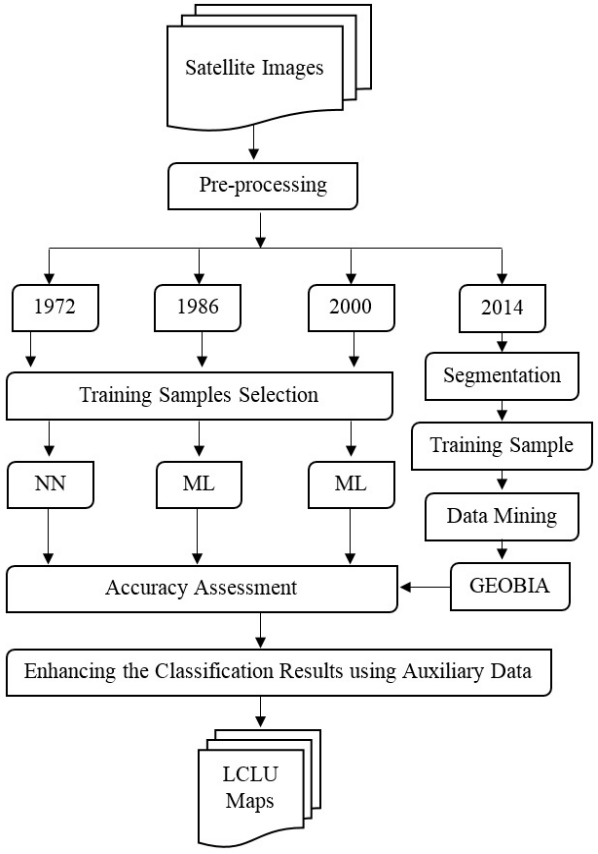

Figure 1. LCLU mapping flowchart. NN = Neural Network, ML = Maximum Likelihood, GEOBIA = Geographic Object-Based Image Analysis.

2.2. Datasets

When selecting the most appropriate remote-sensing images to use, a number of factors such as the complexity of the area, coverage, the study's objectives, user requirements and data availability needed to be considered [20]. The consideration of these factors led to the use of four multi-temporal cloud free L1T Landsat MSS, TM, ETM+ and OLI/TIRS images (Path/Row 162/34) covering the period 1972 to 2014, eventually distributed by the Land Processes Distributed Active Archive Center (LP DAAC) as the core LCLU classification data. In addition, to support the classification, some auxiliary data were used alongside the Landsat data, as shown in Table 1. Google Earth, Yahoo and Bing satellite images offer some advantages in terms of classification, though it should be mentioned that in different areas of the GW, each of these data sources provided distinctive images depending on the time and spatial resolution of the images available. As a result, we used all of these sources together at the same time to increase accuracy. Moreover, a field trip was carried out in May 2013 to collect GCPs and better understand the study area on the ground.

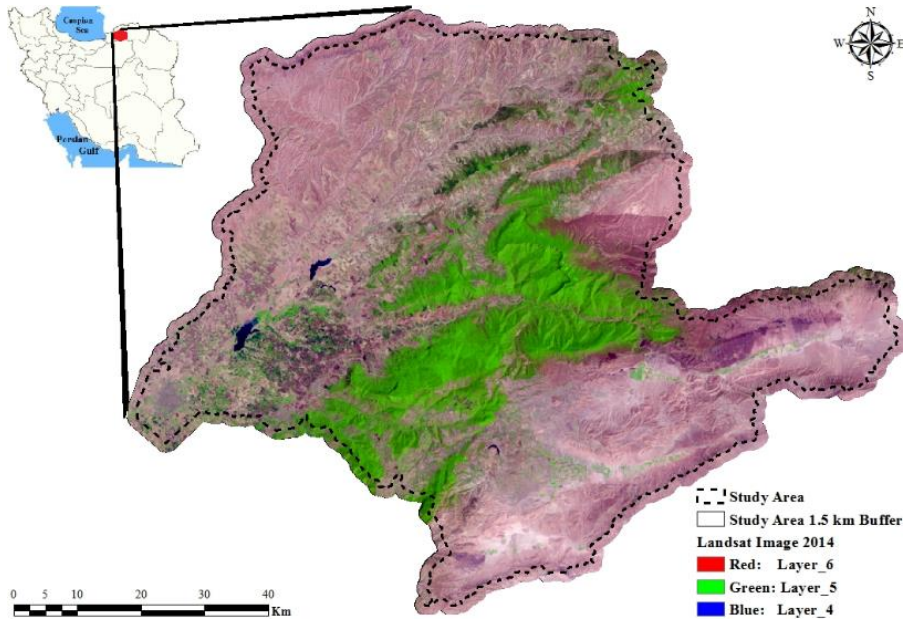

Figure 2. Study area in the northeast of Iran.

Table 1. Data used for the LCLU mapping process.

Data Name	Acquisition Date	Resolution	Full Area Coverage	Source
Landsat/MSS	20 September 1972	60 m	Yes	http://earthexplorer.usgs.gov/
Landsat/TM	19 May 1986	30 m	Yes	http://earthexplorer.usgs.gov/
Landsat ETM+	20 July 2000	30 m (Pan 15)	Yes	http://earthexplorer.usgs.gov/
Landsat OLI/TIRS	19 July 2014	30 m (Pan 15)	Yes	http://earthexplorer.usgs.gov/
Aster	18 July 2001	15 m	No	http://reverb.echo.nasa.gov/
CORONA	27 May 1970	~2.1 m	No	http://earthexplorer.usgs.gov/
Quickbird	2005	0.6 m	No	Geography Department, Ferdowsi University of Mashhad
Aerial Photo	1970	~1.9 m	No	Geography Department, University of Tehran
DEM (Aster)		30 m	Yes	http://earthexplorer.usgs.gov/
Topographic Map			No	Geography Department, University of Tehran
GIS Thematic Maps			Yes/No	Department of Natural Resource and Watershed Management, Golestan
Google/Yahoo/Bing Historical and up to Date Images			Yes/No	Internet

2.3. Image Preprocessing and Pan-Sharpening

The four L1T Landsat images were converted to radiance followed by reflectance, using Equations (1) and (2). More details regarding the equations used can be found in publications [21–23].

$$L_\lambda = Gain \times Pixel\ value + offset \quad (1)$$

$$\rho_\lambda = \frac{\pi L_\lambda d^2}{ESUN_\lambda \sin\theta} \quad (2)$$

where: L_λ is the radiance in units of watts/(meter squared * ster * μm); d is the Earth-Sun distance in astronomical units; $ESUN_\lambda$ is the solar irradiance in units of watts/(meter squared * μm) and θ is the sun elevation in degrees.

We also applied a dark object subtraction model [24] on the images using a methodology commonly applied to reduce atmospheric effects [10].

Pan-sharpening techniques are useful for enhancing the process and results of image processing, and help provide a better understanding of the observed earth surface [14,25]. There are numerous pan-sharpening methods to use on satellite images: high pass filter (HPF), modified intensity-hue-saturation (M-IHS), Ehlers and Gram-Schmidt (GS) [25–28]. The GS pan-sharpening method has become one of the most prevalent approaches to use on multispectral lower resolution images [27]; therefore, the images for 2000 and 2014 that had pan bands in this study were pan-sharpened with the GS pan-sharpening algorithm.

2.4. Classification

Remote sensing has become a fundamental source of data in geographical studies (e.g., LCLU change research studies), and various classification methods have been developed to extract information from imageries. These methods can be classified into two main types: pixel-based and object-based methods. Pixel-based methods can be unsupervised (based on cluster analysis) or supervised. The latter group uses statistical (e.g., maximum likelihood) and non-statistical algorithms (e.g., neural networks and support vector machines) [20], and each of these has its own advantages and disadvantages. We applied both of them to the images used in this study and chose those which gave the best output. The object-based classification, meanwhile, is a more recently introduced classification method, and overcomes some of the particular problems encountered with pixel-based classification, such as the salt-and-pepper effect [29]. We used the pixel-based classification method for the 1972 to 2000 images, and the object-based classification method for the 2014 image.

2.4.1. Pixel-Based Classification

When recognizing and mapping LCLU change, it is obviously extremely important to determine the number of LCLU classes, and then use the best method to detect them [10]. With this in mind, based on conditions in the study area and other studies that had used Landsat images, such as [30] and [31], we decided to use six classes, including: built-up areas, farmland, bare land, range land, forests and water bodies. These six classes were subsequently used with both the pixel-based and object-based classification methods.

A total of 396 patches were collected, including 240 samples for training and 156 samples for validation. For each of these classes, training areas were carefully selected in the different band combination color composites of each image using different sources including field GCPs, CORONA, QuickBird, Aster images, aerial photos and topographic maps, with Google Earth, Yahoo and Bing satellite maps used as references. Afterwards, the training samples selected were tested for separability, to see how well separated they were. The separation results came out between 0 and 2 for a comparison of each couple, with a very good separation characterized by a value of 1.9 to 2, and a very low separation represented by a value of less than 1 [10].

Supervised classifications, using the maximum likelihood, neural network, support vector machine and other classifiers, were carried out on the images as soon as the classification and training sample grouping had been finalized. After that, we checked the accuracy of the classification results based on the overall accuracy, to assess the quality of the classified images. For this accuracy assessment, different randomly well-distributed samples were collected from the previously mentioned auxiliary data sources, plus a confusion matrix was used to provide accuracy measurements, before selecting the best classification output. Table 2 shows the selected classifier algorithms for each image.

Table 2. Selected classifiers for each image.

Image	Classification Method	Classifier
1972	Pixel-based	Neural Network
1986	Pixel-based	Maximum Likelihood
2000	Pixel-based	Maximum Likelihood
2014	Object-Based	Rule-based

To implement the neural network classifier for the 1972 image, we kept constant the training threshold contribution, rate, momentum and interactions at 0.9, 0.2, 0.9 and 1000, respectively. In contrast, we tried different activation functions (logistic and hyperbolic) and changed the number of hidden layers (one and two, according to [10]). Finally, the combination of constant elements and a hidden layer and logistic function provided the best result.

2.4.2. Geographic Object Based Image Analysis

Over the last two decades, advances in earth observation sensors, computer technology and GI science have led to the development of Geographic Object-Based Image Analysis (GEOBIA) as an alternative to the traditional pixel-based image analysis method [32,33]. In [34] they said that "GEOBIA is a systematic framework for geographic object identification, which combines pixels with the same semantic information into an object, thereby generating an integrated geographic object." GEOBIA is a newly developed area of Geographic Information Science and remote sensing in which the automatic segmentation of images into objects of similar spectral, temporal and spatial characteristics is carried out [35]. In contrast to traditional image analysis, GEOBIA works more like the human eye–brain combination [33]. The latter compares an object's properties such as color, square fit, texture, shape and occurrence with other image objects, along with many other properties, to interpret and analyze what the human eye sees [33,35].

Segmentation

GEOBIA starts by segmenting the image grouping pixels into objects, then uses a wide range of object properties to classify the objects or extract object properties from the image [33,36,37]. Multi-resolution segmentation is a popular method of segmentation in the remote-sensing field [36]. To create objects from pixels, some parameters are particularly important, including scale, color and shape, as is the shape's compactness and smoothness [4]. In most studies to date, the selection of parameter values has been done on a trial and error basis [4]. However, we used the ESP tool [38] to calculate the preferred size of the scale parameters. Different values were tested with regard to different geographical object classes, with the optimal values selected based on scale, shape and compactness at 75, 0.5 and 0.9, respectively. The objects created based on these settings were used for further analysis. For more details on segmentation parameters, we refer readers to a range of studies, including [29,39–41].

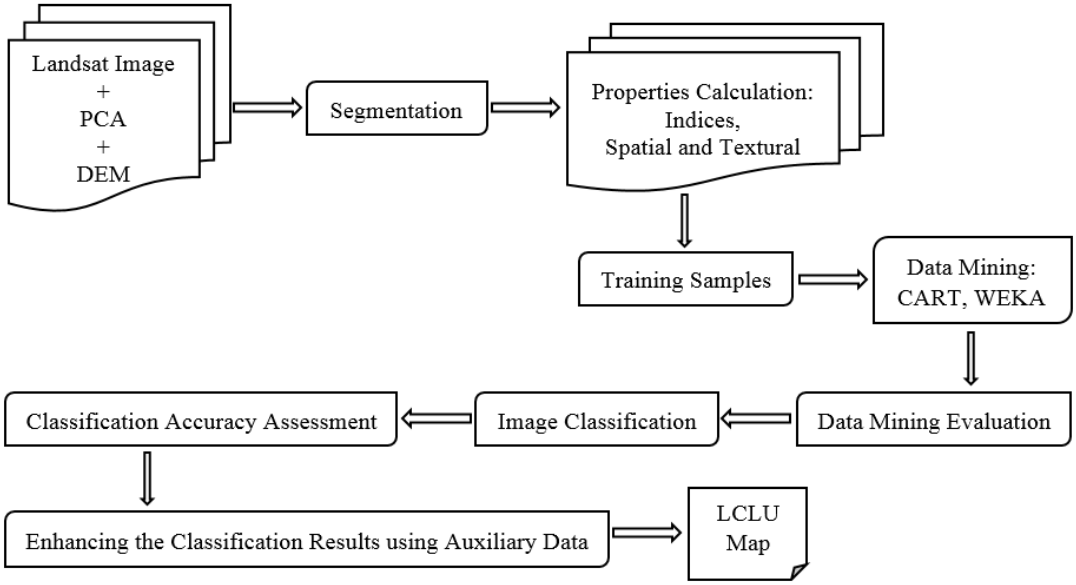

Figure 3. GEOBIA and data-mining procedure flowchart.

Data Mining

Generally, the steps followed during a data-mining exercise include image segmentation, training object sampling, data mining of the samples, an evaluation of the output of data-mining activities, image classification, and then a classification accuracy assessment. The whole process is graphically presented in Figure 3.

To provide inputs for the data mining used in this study, section segmentation was applied to the datasets. After that, the data were parameterized based on the LCLU classification requirements. To detect different classes in the image and prepare good criteria for the data-mining process, we calculated Brightness, the Max.diff index ("the absolute difference between the minimum object mean and the maximum object mean divided by the mean object brightness" [36]), and different indices such as NDVI, NDGRVI, NDBI, GNDVI, LWM, NDMI and SLAVI from the 2014 image, plus carried out principal component analysis (PCA). Slope and aspects were derived from the Digital Elevation Model (DEM). The different spatial, textural and spectral characteristics of the objects used as part of the data-mining process (115 properties) were developed, as shown in Table 3.

Table 3. Characteristics of the objects and indices used as part to the data mining process (STDDEV: Standard Deviation; TC: Tasseled Cap; SLAVI: Specific Leaf Area Vegetation Index; NDVI: Normalized Difference Vegetation Index; NDMI: Normalized Dry Matter Index; NDGRVI: Normalized Difference Green Red Vegetation Index; NDBI: Normalized Difference Build-Up Index; LWM: Land and Water Mask; GNDVI: Green Normalized Difference Vegetation Index).

Name of Attributes	Name of Attributes	Name of Attributes
Mean and STDDEV of B1	Mean and STDDEV of B5-OVER-B4	Brightness
Mean and STDDEV of B2	Mean and STDDEV of B4-OVER-B6	Max Diff
Mean and STDDEV of B3	Mean and STDDEV of B4-OVER-B5	Modified mean brightness
Mean and STDDEV of B4	Mean and STDDEV of B3-OVER-B4	Elliptic fit
Mean and STDDEV of B5	Mean and STDDEV of DEM	Compactness
Mean and STDDEV of B6	Mean and STDDEV of ASPECT	Width
Mean and STDDEV of B7	Mean and STDDEV of SLOPE	Asymmetry
Mean and STDDEV of B8	STDDEV of area represented by segments	Density
Mean and STDDEV of B9	Length width only main line	Rectangular fit
Mean and STDDEV of PCA1	Relative border to image border	Length
Mean and STDDEV of PCA2	Average area represented by segment	Length width
Mean and STDDEV of PCA3	STDDEV curvature only main line	Average branch length
Mean and STDDEV of PCA4	Length of longest edge (polygon)	Volume
Mean and STDDEV of PCA5	Average length of edges (polygon)	Perimeter (polygon)
Mean and STDDEV of PCA6	Polygon self-intersection (polygon)	Length thickness
Mean and STDDEV of PCA7	Radius of smallest enclosing ellipse	Shape index
Mean and STDDEV of TC Wetness	Area excluding inner polygons	Thickness
Mean and STDDEV of TC Greenness	Length of main line regarding cycles	Number of segments
Mean and STDDEV of TC Brightness	Area including inner polygons	Maximum branch length
Mean and STDDEV of SLAVI	Number of inner objects (polygon)	Area
Mean and STDDEV of NDVI	STDDEV of length of edges (polygon)	Border index
Mean and STDDEV of NDMI	Radius of largest enclosed ellipse	Width only main line
Mean and STDDEV of NDGRVI	Degree of skeleton branching	Compactness (polygon)
Mean and STDDEV of NDBI	Length of main line no cycle	Number of pixels
Mean and STDDEV of LWM	Curvature length only main line	Roundness
Mean and STDDEV of GNDVI	Border Length	Main direction
Mean and STDDEV of B7-OVER-B3	Number of edges (polygon)	

Subsequently, the 4495 samples were divided into different land classes, these being: bare land, built-up area, farmland, forest land, range land and water bodies. These classes were chosen to provide classification rule-sets for the data miners.

Rule-sets play an important role in the classification of remote-sensing data used in GEOBIA. The data-mining section of the analysis involves the choice and use of intelligent techniques in order to identify and extract patterns of interest of use in the effective production of knowledge [42], where knowledge is understood to mean the behavior patterns identified for each class of interest. We used two data-mining packages: WEKA (Waikato Environment for Knowledge Analysis) [43] and CART (Classification and Regression Trees) [44–46] to mine the data and create a rule set for this research.

CART is a non-parametric method that uses a systematic procedure to find ripping rules [47]. It includes seven single-variable splitting criteria: Gini, Sym-Gini, Twoing, Ordered Twoing, Class Probability for classification trees, Least Squares and Least Absolute Deviation for regression trees, and

also one multi-variable splitting criterion–the Linear Combinations method [46]. The Gini splitting criteria is the default method. Twoing; meanwhile, is a unique part of the CART method that is normally used for computer modeling, and is suitable for use with classification problems in which there are many classes [46,47]. More details of CART can be found in the studies by [44–48].

The J48 decision tree algorithm was applied here using Waikato Environment for Knowledge Analysis (WEKA), which uses a collection of machine-learning algorithms for its data-mining procedures [42,43,49,50]. The J48 algorithm represents an implementation of C4.5 which selects a property to divide the data into two sub-groups based on the highest normalized information gain (difference in the concept of information entropy). Procedure replication is then applied to each subset until all the cases in each subset fit to the same class. As a result, this procedure creates a leaf node in the decision tree [42,51]. More comprehensive details of the WEKA and J48 applications can be found in [42,43,49,50,52].

To establish the best knowledge model, we evaluated the data-mining results using a standard statistics tool to carry out cross-validation. k-fold cross-validation entails separating a dataset into k accidentally complementary subsets [42]. We used a 10-fold cross-validation process among the training samples, with 10% of the data used for testing and 90% for training. Afterward, the prepared rule set by the machine-learning algorithms were applied to the images. As part of a quality assessment, the accuracy of the classification results was checked based on the overall accuracy, quantity disagreement and allocation disagreement indexes [53].

Although at the end of the classification and accuracy assessment process the LCLU maps created were acceptable, using the auxiliary data we tried to increase the quality of the classification as much as possible through post-processing.

2.5. Accuracy Assessment

As has already been noted, the LCLU maps produced from the pixel- and object-based classifications were assessed for their accuracy. To do so, then, in addition to their overall accuracy assessed based on [53] quantity disagreement and allocation disagreement indexes, other more appropriate statistical tests were also selected and implemented, both for the maps and the reference samples [54]. These indexes were seen as more appropriate because they are able to consider the affiliation between the appropriateness of test samples, as well as their categories and area [54]. According to [53], quantity disagreement is the value of alteration among reference samples and a created map, due to the less-than-optimum match in the proportions of the classes. Allocation disagreement, however, is the amount of spatial deviation seen among classified class pixels taken from validation samples [53,55]. In this study, for the pixel-based classification, 156 samples were selected for each image. For the object-based classification, more than 150 random, well-distributed samples were selected, the samples having been obtained from information gathered during field visits and from all other previously mentioned auxiliary data. For example, using photo interpretation, CORONA satellite images, historical aerial photos and also old topographic maps proved useful for the 1972 and 1986 test samples. For 2000 and 2014, meanwhile, QuickBird and Aster satellite images, along with historical and up-to-date satellite images taken from Google Earth, Yahoo and Bing, provided useful information during the sample selection process.

3. Results and Discussion

3.1. Pixel-Based classification

There were 156 well-distributed random samples used as ground-based data to measure the accuracy of the classification. Figure 4 shows the results of the 1972, 1986 and 2000 image classification processes. The results of the accuracy assessment process for the classifications, including quantity and allocation disagreements and overall accuracy levels, are provided in Table 4. As can be seen from the table, the overall accuracy of the maps ranged from 89.8% for 1986 to 95.9% for 1972. The

quantity disagreement for 1972—that is, the difference between the number of pixels in the reference map and in a comparison map—was 2.4%, while for 1986 and 2000, it was around 6%. Meanwhile, the allocation disagreement related to the spatial classification difference among categories ranged from 2.2% to 2.7%. The results shown in Table 4 indicate that the accuracy of the spatial classification was more than the quantitative accuracy. Nevertheless, visual interpretation was integrated into the classification results within the GIS environment, to enhance the quality of the final maps.

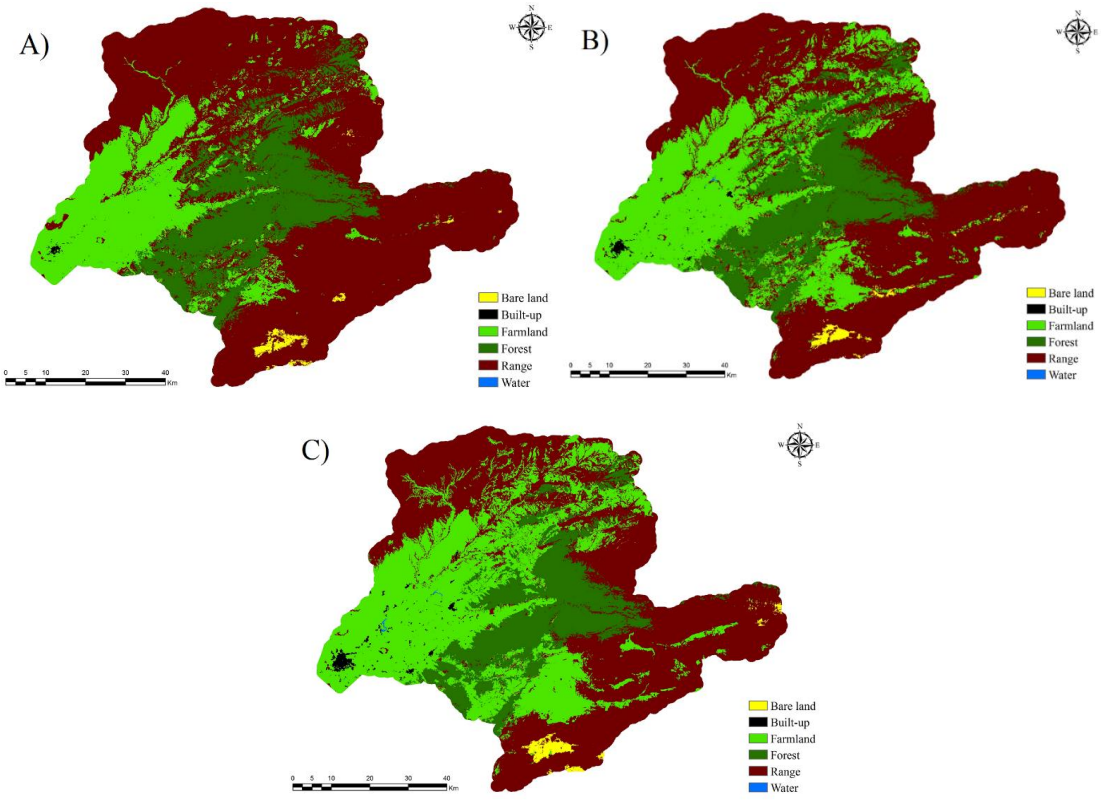

Figure 4. Classification results for: (A) 1972; (B) 1986 and (C) 2000.

Table 4. Selected classifiers for each image as well as the overall accuracy, quantity and allocation disagreement statistics.

Image	Classifier	Overall Accuracy	Quantity Disagreement (%)	Allocation Disagreement (%)
1972	Neural Network	95.9	2.4	2.2
1986	Maximum Likelihood	89.8	6.6	2.5
2000	Maximum Likelihood	91.3	6	2.7

3.2. GEOBIA Classification

Data-mining tools processed the data and detected those attributes deemed important for the building of decision trees. The attributes detected are listed in Table 5.

Applying Gini and J48 algorithms to the training set data presented in Table 3 and using CART and WEKA machine-learning tools allowed the authors to develop decision trees based on the attributes listed in Table 5. Figure 5, meanwhile, shows the decision trees generated by CART and WEKA. To produce precise decision trees, cross-validation was applied during the data-mining process. The overall accuracy of the CART and WEKA data was 96.21% and 96.92%, respectively. As is clear, such

levels of accuracy were acceptable, so the results were evaluated after applying decision trees to the 2014 image.

Table 5. Attributes detected by CART and WEKA.

Attributes	CART	WEKA	Attributes	CART	WEKA
STDDEV of B1	√	√	Mean and STDDEV of B6	√	-
Mean of B8	√	√	Mean and STDDEV of PCA6	√	√
STDDEV of B9	√	√	Mean and STDDEV of TC Greenness	√	√
STDDEV of PCA1	√	-	Mean of B3-OVER-B4	√	√
STDDEV of PCA3	√	√	Mean and STDDEV of DEM	√	√
Mean of PCA4	√	√	STDDEV of ASPECT	√	-
Mean of PCA5	√	√	Average area represented by segment	√	-
STDDEV of PCA5	√	-	Length of longest edge (polygon)	√	√
Mean of PCA7	√	√	Average length of edges (polygon)	√	√
STDDEV of PCA7	-	√	Mean and STDDEV of NDGRVI	-	√
STDDEV of SLAVI	√	√	Brightness	√	√
Mean of NDMI	√	√	Max Diff	√	√
Mean of GNDVI	√	√	Modified mean brightness	√	√
Mean of SLOPE	√	√	Border Length	√	-
Mean of TC Wetness	-	√	Mean of B7	-	√
Asymmetry	-	√	Mean of NDVI	-	√
Mean LWM	-	√			

The accuracy of the results was evaluated by creating a confusion matrix, for which 150 randomly distributed and separate samples were used. The results of this process are presented in Table 6. It can be seen from the data in Table 6 that the overall accuracy of the maps was similar, as both attained 94% accuracy. The quantity disagreement shown for WEKA was 2.1%, while when using CART it was 3.5%. Meanwhile, the allocation disagreement was 2.1% for WEKA and 2.5% for CART. As shown in Table 6, both methods revealed the same level of overall accuracy and thus could be considered acceptable. In the end, the WEKA output—due to better allocation and quantity accuracy—was selected and the post-processing corrections applied to provide a more accurate final LCLU map for 2014 (Figure 6).

Both the pixel-based and object-based methods have advantages and disadvantages. The "salt-and-paper issue" plays a significant role in the pixel-based classification methodology, whereas the rule construction process within GEOBIA analysis is often difficult to perform. However, for the object-based method, its machine-learning and data-mining abilities facilitate rule creation and subsequently image classification. A comparison of the two classification methods reveals that the range of overall accuracy variation in the two object-based classifications is less than three pixel-based ones. Moreover, quantity disagreement for the pixel-based classification method is greater than when using the object-based approach. Nonetheless, allocation disagreement levels for both methods are approximately within the same range.

The results of the classification process for each year provided an overall estimate of LCLU distribution in the study area. As shown in Figures 4 and 6 and as can be seen clearly in Table 7, different classes covered different areas over the years involved. It is apparent from the tables and figures that in 1972, 1986 and 2000, rangeland was the dominant land cover type, covering ~60%, 50% and 45% of the area, respectively. Farmland and forest expanded the most over the period 1972 to 2000, following the LC range. From Table 7, a significant difference can be seen between 2014 and previous years, because rangeland stopped being the most dominant land cover, having been replaced by farmland (40%). In 2014, farmland, rangeland and then forestland were the most dominant land cover types, in that order. Over the whole period, water bodies and built-up land covered the smallest areas (maximums of 1.45% and 0.19%, respectively).

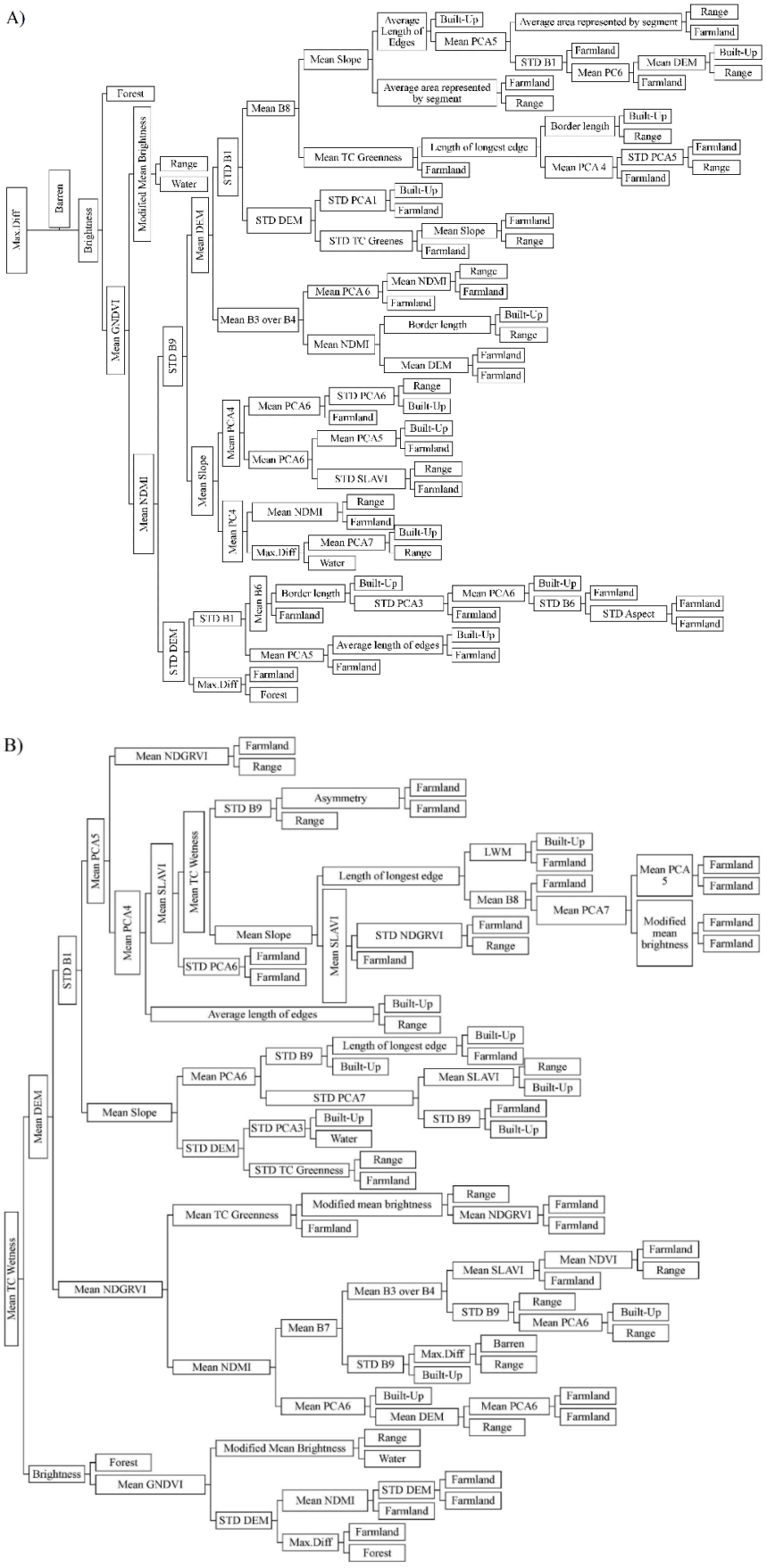

Figure 5. Schematic decision trees created using the data-mining tools (**A**) CART and (**B**) WEKA.

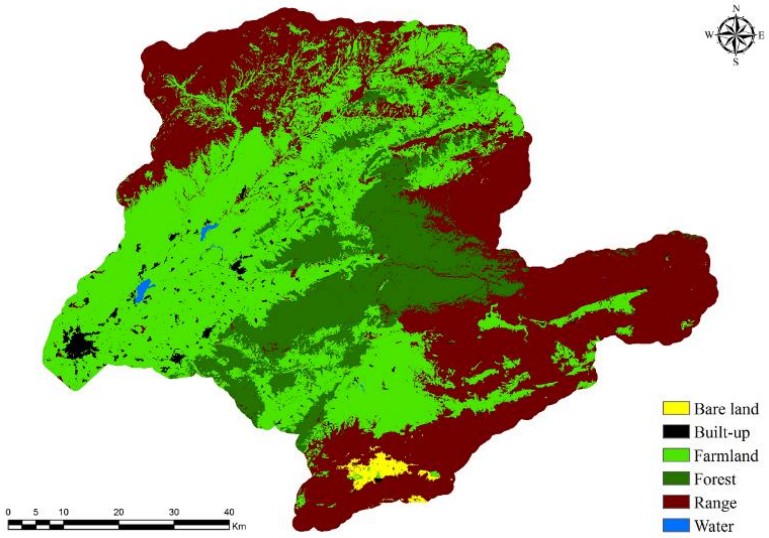

Figure 6. LCLU 2014 classification results.

Table 6. Overall accuracy plus quantity and allocation disagreement statistics for the image classification using the two data-mining methods.

Image	Data Miner	Overall Accuracy	Quantity Disagreement (%)	Allocation Disagreement (%)
2014	WEKA (J48)	94.05	2.1	2.1
2014	CART (GINI)	94.03	3.5	2.5

Table 7. Summary of land cover type areas over the study years—per hectare and as a percentage of the total area.

LCLU Class	1972		1986		2000		2014	
	Area (ha)	(%)	Area (ha)	(%)	Area (ha)	(%)	Area (ha)	(%)
Bare Land	4404.78	0.70	4084.52	0.65	5759.80	0.92	4305.24	0.69
Built-up	819.07	0.13	2646.88	0.42	5050.67	0.81	9057.29	1.45
Farmland	125,379.09	20.02	182,633.27	29.16	224,809.31	35.90	255,753.59	40.84
Forest	122,614.20	19.58	119,333.86	19.06	106,020.83	16.93	106,267.82	16.97
Range	372,998.45	59.56	317,440.78	50.69	284,351.40	45.41	249,663.40	39.87
Water	20.57	0.00	96.95	0.02	244.28	0.04	1,188.97	0.19

From 1972 to 2014, rangeland, the most prevalent class, was largely converted into farmland (more than 26 million ha) and forest (~2 million ha). The latter conversion can be linked to the establishment of the Golestan National Park and the provision of different energy resources for the local population, as well as to reforestation and afforestation activities. Furthermore, during these years, about 5 million ha of forest surface that had for the most part been located close to built-up and flat land were also converted to farmland. Farmland surfaces were mainly converted to built-up areas (approximately 1.3 million ha) and water bodies (more than 200,000 ha); such changes were concentrated in parts of the region covered by plains. However, the expansion of built-up areas was not only to the detriment of farmland; it also took around 465,000 ha from rangelands and 30,000 ha from forests over the period 1972 to 2014. At the same time, barren areas expanded by taking approximately 456,000 ha from rangelands (Table 8). Similarly, [13] who studied tree cover changes during 1987–2001 in part of the study area, found that the forest areas had decreased.

Table 8. Transmission matrix for LCLU changes (ha) over the 1972–2014 period.

1972/2014	Bareland	Built-Up	Farmland	Forest	Range	Water
Bare Land	510,780.94	11,091.94	108,636.19	0.00	360,566.44	0.00
Built-Up	0.00	183,500.44	263.25	0.00	0.00	526.50
Farmland	0.00	1,347,779.25	26,545,861.69	17,177.06	71,649.56	227,827.69
Forest	0.00	30,243.38	4,759,347.38	22,014,225.56	782,257.50	2,121.19
Range	457,898.06	465,264.00	26,129,653.31	1,878,855.75	54,959,785.88	33,194.81
Water	0.00	0.00	779.63	0.00	0.00	3,847.50

4. Conclusion

This study set out to determine Land Cover/Land Use (LCLU) statuses over the period 1972 to 2014 (a period of 42 years) for the Gorganrood watershed in the northeast of Iran. Based on pixel-based remote-sensing and supervised classifications, and including the use of neural network and maximum likelihood methods, the authors created land use maps for the period 1972 to 2000. After that, a combination of GEOBIA remote-sensing and data-mining methods provided the framework needed for the LCLU mapping process to take place, and this was then also applied to a 2014 image. Both pixel-based and object-based classification methods have both advantages and disadvantages. For example, pixel-based classifications suffer from the salt-and-paper problem, while performing rule construction activities using GEOBIA analysis is often difficult. However, using data mining with the object-based method can facilitate rule-set creation and subsequently image classification, and provide a stable level of accuracy in different classifications.

With the LCLU maps obtained, the authors were able to clarify LCLU status over the study period, showing that in 1972, 1986 and 2000, rangeland was the dominant land cover type. Meanwhile, farmland and forestland expanded the most over the period, following the LC range. There was a significant difference found between 2014 and the previous dates tested, as by this time rangeland was no longer the dominant land cover type, having been replaced by farmland, followed by rangeland and then forestland. Over the whole period, water bodies and built-up land covered the smallest areas.

The results of this study indicate that a significant amount of change has occurred in the watershed since 1972, and that this had effect on the area's ecosystems and human livelihoods. In the Gorganrood watershed flood, landslide and land subsidence are dominant natural hazards and, based on the various influences of LCLU on these processes, increases in farmland and built-up areas, in addition to decreases in forestland and rangeland, may well have increased the number and type of natural hazards, especially floods, as flooding predominates in the region. The local and national governments and decision makers can use the study outcomes to understand the nature and location of the LCLU changes that have occurred, and consider these changes when developing future plans and projects to mitigate natural hazards. Using the improved knowledge of LCLU statuses in the area generated by this study, it is recommended that more research be carried out in order to understand the dynamics of and relations among LCLU classes, so that the watershed can be managed more effectively in the future. Also, further studies regarding the impact of LCLU changes on the future of the watershed should be considered, to help improve our knowledge in this area and help manage the future more efficiently.

Acknowledgments: Images were retrieved from the online Data Pool, courtesy of the NASA Land Processes Distributed Active Archive Center (LP DAAC), and the USGS/Earth Resources Observation and Science (EROS) Center in Sioux Falls, South Dakota (https://lpdaac.usgs.gov/data_access/data_pool). In addition, we appreciate the help provided by Seyed Reza Hosseinzadeh and Sajad Bagheri. We are grateful for the constructive comments given by Robert Gilmore Pontius, Jr. and the three anonymous reviewers of our paper.

Author Contributions: Masoud Minaei came up with the research idea and Wolfgang Kainz provided guidance on the overall project. The study was carried out and the initial version of the paper was written by Masoud Minaei. Wolfgang Kainz supervised the entire research, provided valuable advice and made key modifications to the paper. The paper was revised by both.

Conflicts of Interest: The authors declare no conflict of interest.

References

1. Thilagavathi, N.; Subramani, T.; Suresh, M. Land use/land cover change detection analysis in Salem Chalk Hills, South India using remote sensing and GIS. *Disaster Adv.* **2015**, *8*, 44–52.
2. Adhikari, S.; Southworth, J.; Nagendra, H. Understanding forest loss and recovery: A spatiotemporal analysis of land change in and around Bannerghatta National Park, India. *J. Land Use Sci.* **2014**, *10*, 1–23. [CrossRef]
3. Lambin, E.F.; Turner, B.L.; Geist, H.J; Agbola, S.B.; Angelsen, A.; Bruce, J.W.; Coomes, O.T.; Dirzo, R.; Fischer, J.; Folke, C.; *et al.* The causes of land-use and land-cover change: Moving beyond the myths. *Glob. Environ. Chang.* **2001**, *11*, 261–269. [CrossRef]
4. Dingle Robertson, L.; King, D.J. Comparison of pixel- and object-based classification in land cover change mapping. *Int. J. Remote Sens.* **2011**, *32*, 1505–1529. [CrossRef]
5. Chapin Iii, F.S.; Zavaleta, E.S.; Eviner, V.T.; Naylor, R.L.; Vitousek, P.M.; Reynolds, H.L.; Hooper, D.U.; Lavorel, S.; Sala, O.E.; Hobbie, S.E.; *et al.* Consequences of changing biodiversity. *Nature* **2000**, *405*, 234–242. [CrossRef] [PubMed]
6. Berakhi, R.O.; Oyana, T.J.; Adu-Prah, S. Land use and land cover change and its implications in Kagera river basin, East Africa. *Afr. Geogr. Rev.* **2014**, *34*, 1–23. [CrossRef]
7. Statistical-Center-of-Iran. *Iranian Population and Housing Census 1385—Golestan Province General Results*; Statistical-Center-of-Iran: Tehran, Iran, 2006.
8. Qin, Y.; Niu, Z.; Chen, F.; Li, B.; Ban, Y. Object-based land cover change detection for cross-sensor images. *Int. J. Remote Sens.* **2013**, *34*, 6723–6737. [CrossRef]
9. Yesmin, R.; Mohiuddin, A.S.M.; Uddin, M.J.; Shahid, M.A. Land use and land cover change detection at Mirzapur Union of Gazipur District of Bangladesh using remote sensing and GIS technology. In Proceedings of the IOP Conference Series: Earth and Environmental Science, Kuala Lumpur, Malaysia, 22–23 April 2014.
10. Kolios, S.; Stylios, C.D. Identification of land cover/land use changes in the greater area of the Preveza peninsula in Greece using Landsat satellite data. *Appl. Geogr.* **2013**, *40*, 150–160. [CrossRef]
11. Abd El-Kawy, O.R.; Rød, J.K.; Ismail, H.A.; Suliman, A.S. Land use and land cover change detection in the western Nile delta of Egypt using remote sensing data. *Appl. Geogr.* **2011**, *31*, 483–494. [CrossRef]
12. Yang, X.; Lo, C.P. Using a time series of satellite imagery to detect land use and land cover changes in the Atlanta, Georgia metropolitan area. *Int. J. Remote Sens.* **2002**, *23*, 1775–1798. [CrossRef]
13. Salman Mahini, A.; Feghhi, J.; Nadali, A.; Riazi, B. Tree cover change detection through Artificial Neural Network classification using Landsat TM and ETM+ images (case study: Golestan Province, Iran). *Iran. J. For. Poplar Res.* **2008**, *16*, 495–505.
14. Saadat, H.; Adamowski, J.; Bonnell, R.; Sharifi, F.; Namdar, M.; Ale-Ebrahim, S. Land use and land cover classification over a large area in Iran based on single date analysis of satellite imagery. *ISPRS J. Photogramm. Remote Sens.* **2011**, *66*, 608–619. [CrossRef]
15. Abbaszadeh Tehrani, N.; Makhdoum, M.F.; Mahdavi, M. Studying the impacts of land use changes on flood flows by using remote sensing(RS) and geographical information system (GIS) techniques—A case study in dough river watershed, Northeast of Iran. *Environ. Res.* **2011**, *1*, 1–14.
16. Mallinis, G.; Koutsias, N.; Arianoutsou, M. Monitoring land use/land cover transformations from 1945 to 2007 in two peri-urban mountainous areas of Athens metropolitan area, Greece. *Sci. Total Environ.* **2014**, *490*, 262–278. [CrossRef] [PubMed]
17. Lu, D.; Mausel, P.; Brondízio, E.; Moran, E. Change detection techniques. *Int. J. Remote Sens.* **2004**, *25*, 2365–2401. [CrossRef]
18. Mohammadi, J.; Shataee, S. Possibility investigation of tree diversity mapping using Landsat ETM+ data in the Hyrcanian forests of Iran. *Remote Sens. Environ.* **2010**, *114*, 1504–1512. [CrossRef]
19. Delbari, M.; Afrasiab, P.; Jahani, S. Spatial interpolation of monthly and annual rainfall in northeast of Iran. *Meteorol. Atmos. Phys.* **2013**, *122*, 103–113. [CrossRef]
20. Lu, D.S.; Li, G.Y.; Kuang, W.H.; Moran, E. Methods to extract impervious surface areas from satellite images. *Int. J. Digit. Earth* **2014**, *7*, 93–112. [CrossRef]
21. USGS. Using the USGS Landsat 8 Product. Available online: http://landsat.usgs.gov/Landsat8_Using_Product.php (accessed on 10 March 2015).

22. USGS. How is Radiance Calculated? Available online: http://landsat.usgs.gov/how_is_radiance_calculated.php (accessed on 12 March 2016).
23. Exelis VIS, p.d.c. Radiometric Calibration. Available online: http://www.exelisvis.com/docs/RadiometricCalibration.html (accessed on 12 March 2016).
24. Chavez, P.S. Radiometric calibration of Landsat thematic mapper multispectral images. *Photogramm. Eng. Remote Sens.* **1989**, *55*, 1285–1294.
25. Yuhendra; Alimuddin, I.; Sumantyo, J.T.S.; Kuze, H. Assessment of pan-sharpening methods applied to image fusion of remotely sensed multi-band data. *Int. J. Appl. Earth Obs. Geoinform.* **2012**, *18*, 165–175. [CrossRef]
26. ArcGIS Help. Fundamentals of Panchromatic Sharpening. Available online: http://resources.arcgis.com/en/help/main/10.1/index.html#//009t000000mw000000 (accessed on 11 March 2015).
27. Maurer, T. How to pan-sharpen images using the Gram-Schmidt pan-sharpen method-a recipe. *Int. Arch. Photogramm. Remote Sens. Spat. Inf. Sci.* **2013**, *XL-1/W1*, 239–244. [CrossRef]
28. Laben, C.A.; Brower, B.V. Process for Enhancing the Spatial Resolution of Multispectral Imagery using Pan-Sharpening. Google Patents US6011875 A, 2000.
29. Blaschke, T. Object based image analysis for remote sensing. *ISPRS J. Photogramm. Remote Sens.* **2010**, *65*, 2–16. [CrossRef]
30. Nutini, F.; Boschetti, M.; Brivio, P.A.; Bocchi, S.; Antoninetti, M. Land-use and land-cover change detection in a semi-arid area of Niger using multi-temporal analysis of Landsat images. *Int. J. Remote Sens.* **2013**, *34*, 4769–4790. [CrossRef]
31. Wu, G.; Gao, Y.; Wang, Y.; Wang, Y.Y.; Xu, D. Land-use/land cover changes and their driving forces around wetlands in Shangri-La County, Yunnan Province, China. *Int. J. Sustain. Dev. World Ecol.* **2015**, *22*, 110–116. [CrossRef]
32. Gao, Y.; Mas, J.F. A comparison of the performance of pixel based and object based classifications over images with various spatial resolutions. *ISPRS Arch.* **2008**, *XXXVIII-4/C1*, 1–6.
33. Addink, E.A.; van Coillie, F.M.B.; de Jong, S.M. Introduction to the GEOBIA 2010 special issue: From pixels to geographic objects in remote sensing image analysis. *Int. J. Appl. Earth Obs. Geoinf.* **2012**, *15*, 1–6. [CrossRef]
34. Ma, L.; Cheng, L.; Li, M.; Liu, Y.; Ma, X. Training set size, scale, and features in geographic object-based image analysis of very high resolution unmanned aerial vehicle imagery. *ISPRS J. Photogramm. Remote Sens.* **2015**, *102*, 14–27. [CrossRef]
35. Rabia, A.H.; Terribile, F. Semi-automated Classification of gray scale aerial photographs using geographic object based image analysis (GEOBIA) technique. In *European Geosciences Union General Assembly-Geophysical Research Abstracts*; Vienna, Austria, 2013.
36. Blaschke, T.; Feizizadeh, B.; Holbling, D. Object-based image analysis and digital terrain analysis for locating landslides in the urmia lake basin, Iran. *IEEE J. Sel. Top. Appl. Earth Obs. Remote Sens.* **2014**, *7*, 4806–4817. [CrossRef]
37. Witharana, C.; Civco, D.L.; Meyer, T.H. Evaluation of data fusion and image segmentation in earth observation based rapid mapping workflows. *ISPRS J. Photogramm. Remote Sens.* **2014**, *87*, 1–18. [CrossRef]
38. Dragut, L.; Tiede, D.; Levick, S.R. ESP: A tool to estimate scale parameter for multiresolution image segmentation of remotely sensed data. *Int. J. Geogr. Inf. Sci.* **2010**, *24*, 859–871. [CrossRef]
39. Wang, Z.; Jensen, J.R.; Im, J. An automatic region-based image segmentation algorithm for remote sensing applications. *Environ. Model. Softw.* **2010**, *25*, 1149–1165. [CrossRef]
40. Lang, S. Object-based image analysis for remote sensing applications: Modeling reality–dealing with complexity. In *Object-Based Image Analysis*; Blaschke, T., Lang, S., Hay, G., Eds.; Springer: Berlin, Germany, 2008; pp. 3–27.
41. Baatz, M.; Schäpe, M. Multiresolution segmentation. In *Angewandte Geographische Informations-Verarbeitung*; Strobl, J., Blaschke, T., Griesebner, G., Eds.; Wichmann Verlag: Karlsruhe, Germany, 2000; pp. 12–23.
42. Vieira, M.A.; Formaggio, A.R.; Renno, C.D.; Atzberger, C.; Aguiar, D.A.; Mello, M.P. Object based image analysis and data mining applied to a remotely sensed Landsat time-series to map sugarcane over large areas. *Remote Sens. Environ.* **2012**, *123*, 553–562. [CrossRef]
43. Hall, M.; Frank, E.; Holmes, G.; Pfahringer, B.; Reutemann, P.; Witten, I.H. The WEKA data mining software: An update. *SIGKDD Explor. Newslett.* **2009**, *11*, 10–18. [CrossRef]

44. Breiman, L.; Friedman, J.; Olshen, R.; Stone, C. *Classification and Regression Trees*; Pacific Grove: Wadsworth, OH, USA, 1984.
45. Steinberg, D.; Colla, P. *Cart-Classification and Regression Tree*; Salford Systems: San Diego, CA, USA, 1997.
46. Dan Steinberg, M.G. *CART 6.0 User's Manual*; Salford Systems: San Diego, CA, USA, 2006.
47. Waheed, T.; Bonnell, R.B.; Prasher, S.O.; Paulet, E. Measuring performance in precision agriculture: CART—A decision tree approach. *Agric. Water Manag.* **2006**, *84*, 173–185. [CrossRef]
48. Salford System. *CART Classification and Regression Trees*; Salford Systems: San Diego, CA, USA, 2015.
49. Sharma, R.; Ghosh, A.; Joshi, P.K. Decision tree approach for classification of remotely sensed satellite data using open source support. *J. Earth Syst. Sci.* **2013**, *122*, 1237–1247. [CrossRef]
50. Biswal, S.; Ghosh, A.; Sharma, R.; Joshi, P.K. Satellite data classification using open source support. *J. Indian Soc. Remote Sens.* **2013**, *41*, 523–530. [CrossRef]
51. Kramer, S. J48. Available online: http://www.opentox.org/dev/documentation/components/j48/ (accessed on 12 March 2016).
52. Waikato, M.L.G. Weka 3: Data Mining Software in Java. Available online: http://www.cs.waikato.ac.nz/~ml/weka/ (accessed on 12 March 2016).
53. Pontius, R.G., Jr.; Millones, M. Death to Kappa: Birth of quantity disagreement and allocation disagreement for accuracy assessment. *Int. J. Remote Sens.* **2011**, *32*, 4407–4429. [CrossRef]
54. Cordeiro, C.L.D.; Rossetti, D.D. Mapping vegetation in a late quaternary landform of the Amazonian wetlands using object-based image analysis and decision tree classification. *Int. J. Remote Sens.* **2015**, *36*, 3397–3422. [CrossRef]
55. Mansour, K.; Mutanga, O.; Adam, E.; Abdel-Rahman, E.M. Multispectral remote sensing for mapping grassland degradation using the key indicators of grass species and edaphic factors. *Geocarto Int.* **2016**, *31*. [CrossRef]